Bessel vortices in spin-orbit-coupled spin-1 Bose-Einstein condensates

Jun-Zhu Li, Huan-Bo Luo, and Lu Li*

Institute of Theoretical Physics and Department of Physics, State Key Laboratory of Quantum Optics and Quantum Optics Devices, Collaborative Innovation Center of Extreme Optics, Shanxi University, Taiyuan 030006, China

(Received 21 September 2022; accepted 19 December 2022; published 30 December 2022)

We investigate the stationary vortex solutions in two-dimensional Rashba spin-orbit-coupled spin-1 Bose-Einstein condensates. By introducing the generalized momentum operator, the linear version of the system can be solved exactly and its solutions are a set of the Bessel vortices. Based on the linear version solutions, the stationary vortex solutions of the full nonlinear system are constructed and determined entirely by the variational approximation. The results show that the variational results are in good agreement with the numerical ones. By means of the variational results, the vortex ground-state phase transition between the stationary vortex solutions, the stability, and the unit Bloch vector textures are discussed in detail. The results have the potential to be realized in experiment.

DOI: 10.1103/PhysRevA.106.063321

I. INTRODUCTION

Atomic Bose-Einstein condensates (BECs), as an extremely clean quantum system with full controllability, have been used to emulate various effects from condensed-matter systems [1]. A well-known example is the spin-orbit (SO) coupling, which plays an important role in spin Hall effects [2], topological insulators [3], spintronic devices [4], etc. The past decade has witnessed the experimental realization of SO coupling in BECs from one dimension [5,6] to two dimensions [7] (see the reviews of the experimental and theoretical findings in Refs. [8–11]). At the same time, many remarkable characteristics, such as vortices [12–15], skyrmions [16], and solitons [17–28], have been predicted theoretically in the SO-coupled BECs (see also the review in [29]). Also, the SO coupling, as a basic effect, is included also in the study of chiral supersolids [30] and polariton topological insulators [31].

Analytical solutions always play a very important role in understanding the system, explaining various phenomena and making predictions under certain conditions. Generally, in the framework of the variational approximation, the Gaussian ansatz is presupposed in studies of the SO-coupled spin-1 BEC [32,33]. Although the variational method under the Gaussian ansatz is easy to implement, its accuracy and scope of application are limited. Recently, based on the Bessel vortex solutions of the linear version of the system, Josephson oscillations of chirality and Bessel vortices in the SO-coupled spin-$\frac{1}{2}$ BECs have been studied [34,35]. Compared with the Gaussian ansatz, these investigations provide a more accurate way to study the vortex dynamics of the nonlinear system. Inspired by them, we consider the analytical vortex solutions of two-dimensional (2D) SO coupled spin-1 BECs and find some different properties between pseudospin-$\frac{1}{2}$ BECs and spin-1 BECs, including the occurrence of a polar state in SO-coupled spin-1 BECs and their topological properties.

In this paper we first show the analytical solutions of the linear version of spin-1 BECs with the SO coupling by means of the Bessel function. We find that the Bessel vortices are the fundamental solution of the linear version of spin-1 BECs with the SO coupling. In the presence of attractive contact interactions, the Bessel vortex solutions of the linear equation are modified by multiplying a truncation function and the vortex states of the full nonlinear system are determined by means of the variational approximation. All the variational solutions are perfectly matched with the numerical results. With the help of the variational solutions, the phase transition between the vortex ground states, stability, and topological properties are also discussed.

The rest of this paper is structured as follows. In Sec. II the theoretical model is introduced. In Sec. III the linear solution is constructed by means of the Bessel function. Based on the linear vortex solutions, the nonlinear vortex solution is constructed by means of the variational approximation in Sec. IV. At the same time, the vortex ground state of the system, the stability, and the unit Bloch vector textures are discussed in detail. The main results of the paper are summarized in Sec. V.

II. MODEL AND ITS REDUCTIONS

We consider a SO-coupled spin-1 BEC with attractive contact interaction in 2D space. The spinor wave function $\Psi = (\Psi_{+1}, \Psi_0, \Psi_{-1})^T$ of this system can be governed by Gross-Pitaevskii (GP) equations in the dimensionless form

$$i\partial_t \Psi = \left(-\frac{\nabla_\perp^2}{2} + i\beta(F_y\partial_x - F_x\partial_y) + c_0\rho + c_2\rho\mathbf{S}\cdot\mathbf{F}\right)\Psi, \tag{1}$$

*llz@sxu.edu.cn

where β is the SO-coupling strength and $\mathbf{F} = (F_x, F_y, F_z)$ is a vector of spin-1 matrices with

$$F_x = \frac{1}{\sqrt{2}}\begin{pmatrix} 0 & 1 & 0 \\ 1 & 0 & 1 \\ 0 & 1 & 0 \end{pmatrix}, \quad F_y = \frac{1}{\sqrt{2}}\begin{pmatrix} 0 & -i & 0 \\ i & 0 & -i \\ 0 & i & 0 \end{pmatrix}, \quad F_z = \begin{pmatrix} 1 & 0 & 0 \\ 0 & 0 & 0 \\ 0 & 0 & -1 \end{pmatrix}. \tag{2}$$

The coefficients $c_0 < 0$ and $c_2 < 0$ are the strengths of the particle-attraction and spin-attraction contact interactions, respectively. Here $\rho = \Psi^\dagger\Psi$ is the particle density and $\mathbf{S} = \Psi^\dagger\mathbf{F}\Psi/\rho$ is the local spin. Below we set $\beta = 1$ by means of rescaling.

Stationary solutions of Eq. (1) with chemical potential μ are sought in the usual form

$$\Psi(x, y, t) = \psi(x, y)\exp(-i\mu t), \tag{3}$$

with stationary functions $\psi(x, y) = (\psi_{+1}, \psi_0, \psi_{-1})^T$ satisfying the equation

$$\mu\psi = \left(-\frac{\nabla_\perp^2}{2} + i(F_y\partial_x - F_x\partial_y) + c_0\rho + c_2\rho\mathbf{S}\cdot\mathbf{F}\right)\psi. \tag{4}$$

In this paper we seek the stationary vortex solutions for Eq. (4) in the form

$$\begin{aligned} \psi_1(x, y) &= e^{-i(m+1)\theta}R_1(r), \\ \psi_0(x, y) &= e^{-im\theta}R_0(r), \\ \psi_{-1}(x, y) &= e^{-i(m-1)\theta}R_{-1}(r), \end{aligned} \tag{5}$$

where (r, θ) are the polar coordinates, m is an integer winding number, and $R_{1,0,-1}(r)$ are three radial wave functions. Substituting Eq. (5) into Eq. (4) yields

$$\begin{aligned} \mu R_{\pm1} =& -\frac{1}{2}\left(\partial_r^2 + \frac{1}{r}\partial_r - \frac{(m\pm1)^2}{r^2}\right)R_{\pm1} \\ &+ \frac{1}{\sqrt{2}}\left(\pm\partial_r - \frac{m}{r}\right)R_0 + c_0(R_1^2 + R_0^2 + R_{-1}^2)R_{\pm1} \\ &\pm c_2\left(R_1^2 - R_{-1}^2\right)R_{\pm1} + c_2R_0^2(R_{\pm1} + R_{\mp1}), \\ \mu R_0 =& -\frac{1}{2}\left(\partial_r^2 + \frac{1}{r}\partial_r - \frac{m^2}{r^2}\right)R_0 \\ &- \frac{1}{\sqrt{2}}\left[\left(\partial_r + \frac{m+1}{r}\right)R_{+1} - \left(\partial_r - \frac{m-1}{r}\right)R_{-1}\right] \\ &+ c_0\left(R_1^2 + R_0^2 + R_{-1}^2\right)R_0 + c_2(R_1 + R_{-1})^2R_0. \end{aligned} \tag{6}$$

Thus, we can obtain the stationary vortex solutions by solving numerically Eq. (6).

III. EXACT VORTEX STATES OF THE LINEAR VERSION

In the section we consider the stationary vortex solutions of the linear version of Eq. (4), i.e., $\mu\psi = \hat{H}\psi$, with the Hamiltonian

$$\hat{H} = -\frac{\nabla_\perp^2}{2} + i(F_y\partial_x - F_x\partial_y). \tag{7}$$

First, we introduce a generalized momentum operator

$$\hat{P} = iF_x\partial_y - iF_y\partial_x, \tag{8}$$

whose eigenvalue equation $k\psi = \hat{P}\psi$ with real k admits a set of exact eigenstates in the form (5) with

$$R_1 = \frac{J_{m+1}(kr)}{\sqrt{2}}, \quad R_0 = J_m(kr), \quad R_{-1} = \frac{J_{m-1}(kr)}{\sqrt{2}}, \tag{9}$$

where J_m denotes the Bessel function with integer number m and k is the radial momentum.

Next we turn to the eigenvalue problem of the linear Hamiltonian $\hat{H}$. It can be directly shown that the Hamiltonian $\hat{H}$ commutes with the generalized momentum operator $\hat{P}$, i.e., $[\hat{H}, \hat{P}] = 0$. Thus the eigenstate ψ given by Eq. (5) with the expression (9) is also the eigenstate of $\hat{H}$. Also, the Hamiltonian can be written as $\hat{H} = \hat{P}^2/2 - \hat{B}/4 - \hat{P}$, where $\hat{B} = (F_z^2 + F_x^2 - F_y^2)\partial_{xx} + (F_z^2 - F_x^2 + F_y^2)\partial_{yy} + 2(F_xF_y + F_yF_x)\partial_{xy}$ meeting $\hat{B}\psi = 0$, and so the corresponding chemical potential is

$$\mu = \frac{k^2}{2} - k, \tag{10}$$

where the two terms represent the kinetic energy and SO-coupling energy. The chemical potential attains its minimum $\mu_{\min} = -\frac{1}{2}$ at $k = 1$. Thus, the solution (5) with Eq. (9) presents a set of Bessel vortices with winding numbers $-(m + 1)$, $-m$, and $-(m - 1)$ in the ψ_1, ψ_0, and ψ_{-1} components, respectively. Similar exact solutions of the SO-coupled binary linear GP equations were recently reported in Refs. [34,35]. Note that all the vortex states are degenerate with respect to the excitation number m, as μ, given by Eq. (10), does not depend on m.

Naturally, the norm integral for this linear state in the free space diverges as

$$\begin{aligned} N &\equiv N_1 + N_0 + N_{-1} \\ &= \lim_{R\to\infty}\left\{2\pi\int_0^R \left[R_1^2 + R_0^2 + R_{-1}^2\right]r\,dr\right\} \simeq 4R, \end{aligned} \tag{11}$$

while the ratio of the norms of the three components is finite:

$$N_1{:}N_0{:}N_{-1} = 1{:}2{:}1. \tag{12}$$

The linear Bessel vortices indicate that particles propagate radially with momentum k. The fact that the norm diverges means that such states require an infinite number of particles and therefore cannot be realized in the real world. As shown below, taking into account the self-attractive nonlinearity in Eq. (4) makes it possible to replace the vortex states by similar ones, but with a finite norm.

IV. CONSTRUCTION OF NONLINEAR VORTEX STATES

In the following, based on the linear vortex solutions mentioned above and by means of the variational approximation (VA), we construct the stationary vortex solutions of the full nonlinear equation (4). In this process, a reasonable assumption about the ansatz is crucial.

We first consider the asymptotic expression of the vortex solutions for Eq. (4), which should be of the form

$$\begin{aligned} R_1 &\underset{r\to\infty}{\approx} \frac{C}{\sqrt{2r}} e^{-\sqrt{-2\mu-1}r} \sin\left[r - \frac{\pi}{2}\left(m+\frac{1}{2}\right)\right], \\ R_0 &\underset{r\to\infty}{\approx} \frac{C}{\sqrt{r}} e^{-\sqrt{-2\mu-1}r} \cos\left[r - \frac{\pi}{2}\left(m+\frac{1}{2}\right)\right], \\ R_{-1} &\underset{r\to\infty}{\approx} -\frac{C}{\sqrt{2r}} e^{-\sqrt{-2\mu-1}r} \sin\left[r - \frac{\pi}{2}\left(m+\frac{1}{2}\right)\right], \end{aligned} \tag{13}$$

where C is a constant. Indeed, it can be verified that the asymptotic expression (13) is valid by substituting it into Eq. (6) and ignoring an infinitesimal of higher order. Thus, the localized states exist at a value of the chemical potential $\mu < -\frac{1}{2}$ in the nonlinear regime.

The self-focusing nonlinearity chops off the slowly decaying tails of the Bessel wave function, which make its integral norm diverging. To take this effect into account in the framework of the VA, we adopt an ansatz based on the wave function (9), multiplied by truncation factor $A\,\mathrm{sech}(ar)$, with amplitude A and inverse width a,

$$\begin{aligned} R_1(r) &= \frac{A}{\sqrt{2}}\mathrm{sech}(ar) J_{m+1}(kr), \\ R_0(r) &= A\,\mathrm{sech}(ar) J_m(kr), \\ R_{-1}(r) &= \frac{A}{\sqrt{2}}\mathrm{sech}(ar) J_{m-1}(kr), \end{aligned} \tag{14}$$

where k is still the radial momentum because it can be obtained by evaluating expectation value of the generalized momentum operator (8) in the VA function ψ given by Eqs. (5) and (14), i.e., $\iint \psi^\dagger \hat{P}\psi\, dx\, dy / \iint \psi^\dagger \psi\, dx\, dy = k$. The truncation factor $\mathrm{sech}(ar)$ is chosen here and it is easy to prove that the ansatz (14) is compatible with the asymptotic expression (13) at $k = 1$ and $\mu = -(a^2+1)/2$. One can see that $-a^2/2$ is the energy shift from the linear version of the chemical potential $\mu = -\frac{1}{2}$ in the nonlinear case. The amplitude A can be determined, as a function of a and k, by imposing the normalization condition $N = \iint \psi^\dagger \psi\, dx\, dy = 1$.

In order to determine the parameters a and k, we need to minimize the total energy

$$\begin{aligned} E(a,k) = \frac{1}{2}\iint [&-\psi^\dagger \nabla_\perp^2 \psi + 2i\psi^\dagger (F_y \partial_x - F_x \partial_y)\psi \\ &+ c_0 n^2 + c_2 n^2 |\mathbf{S}|^2] dx\, dy. \end{aligned} \tag{15}$$

The expression of the total energy $E(a,k)$ can be expended by the substitution of Eqs. (5) and (14) into Eq. (15) in the polar coordinates, and its minimization can be numerically implemented by means of the simplex search method [36]. This method differs from that used in Refs. [32,33], in which the total energy was exactly calculated by using the Gaussian ansatz. Figure 1 presents the corresponding results for the states with $m = 0, 1$, varying values of c_2 at $c_0 = -1.5$. For the state with $m = 0$, the parameters a and k remain unchanged as c_2 varies from -5 to 0, resulting in the total energy E and amplitude A unchanged too. The result can be interpreted by the fact that $\mathbf{S} = 0$ for the state with $m = 0$. For the state with $m = 1$, it is found that with increasing $|c_2|$, the parameters a and k increase and the total energy E decreases, where the inverse width a increases sharply as $c_2 \to -4.6$ until it becomes infinity at $c_2 = -4.6$, as shown in Fig. 1(a), which means that a collapse occurs [37,38]. Also, one can see from Fig. 1(c) that the total energy of the state with $m = 0$ is less than that of the state with $m = 1$ as $c_2 > -1.2$, and the opposite is true as $c_2 < -1.2$. Thus, for given $c_0 = -1.5$, $c_2 = -1.2$ provides a vortex ground-state phase-transition point, at which the vortex ground state is transformed into the state with $m = 1$ from the state with $m = 0$.

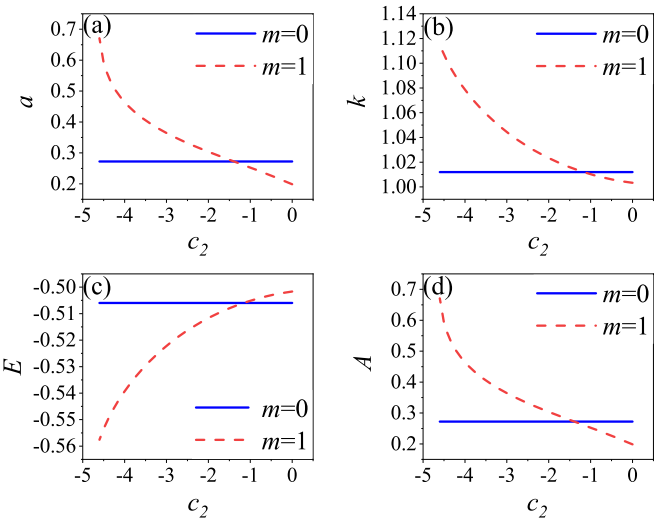

FIG. 1. (a) Inverse width a, (b) momentum k, (c) total energy E, and (d) real amplitude A as a function of interaction strength c_2 at $c_0 = -1.5$. Here the blue solid and red dashed curves correspond to the state with $m = 0$ and 1, respectively.

It should be emphasized that Fig. 1 presents only the results of $c_0 = -1.5$. In general, the diagram of the vortex ground state described by the state with $m = 0$ and the state with $m = 1$ on the (c_0, c_2) plane is shown in Fig. 2. From it one can see that for given a particle-attractive interaction strength

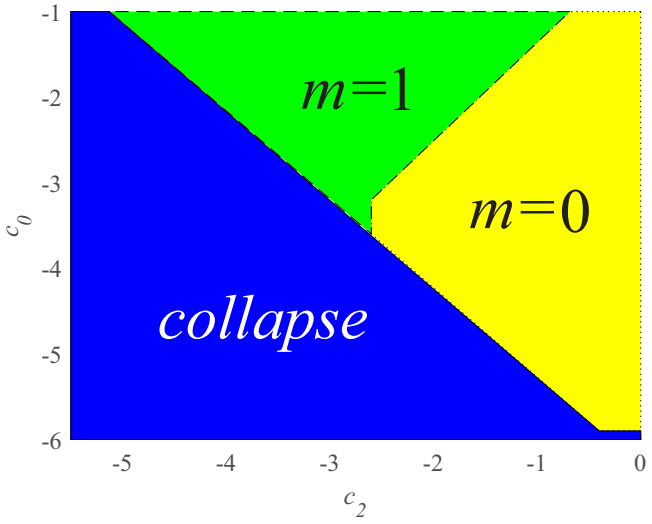

FIG. 2. Diagram of the vortex ground state described by the states with $m = 0$ and 1 on the (c_0, c_2) plane.

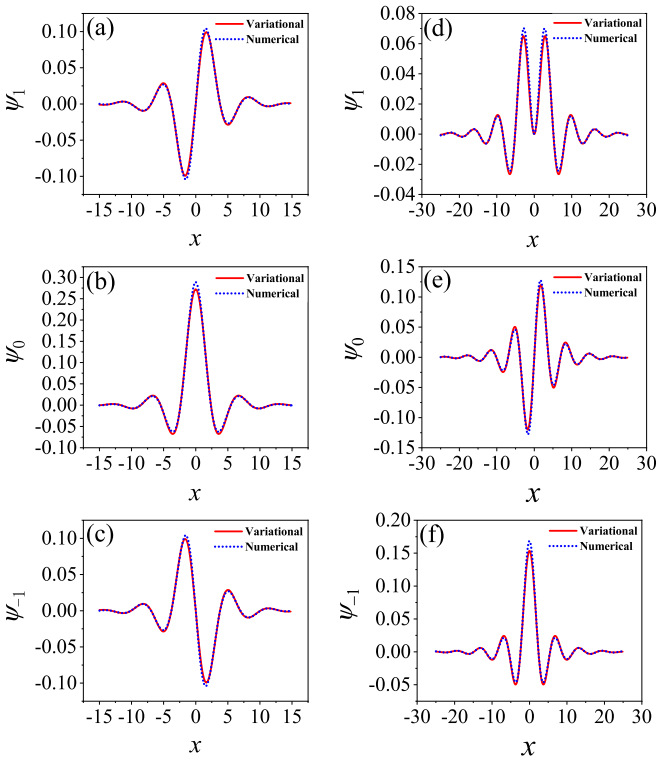

FIG. 3. Distributions of the vortex ground-state wave function at $y = 0$, where (a)–(c) $c_0 = -1.5$, $c_2 = -0.5$, and the blue dotted curves correspond to the state with $m = 0$ and (d)–(f) $c_0 = c_2 = -1$ and the blue dotted curves correspond to the state with $m = 1$.

$c_0 > -3.6$, increasing the spin-attractive interaction strength $|c_2|$ will cause the vortex ground-state phase transition from the state with $m = 0$ to the state with $m = 1$ until collapse. While as $-5.9 < c_0 < -3.6$ the state with $m = 0$, as the vortex ground state, collapses directly with the increase of $|c_2|$, as $c_0 < -5.9$, collapse only occurs for all of c_2 [37–39]. Furthermore, one find that the threshold of $|c_0|$, above which the collapse occurs, will decrease with increasing $|c_2|$. This means that the spin-attraction interaction increases the centripetal velocity of the particles, i.e., the attraction-induced velocity [39].

In order to verify the correctness of the variational results, we solve Eq. (1) numerically by employing the norm-preserving imaginary-time propagation method. As typical examples, Fig. 3 presents the distributions of the vortex ground-state wave function at $y = 0$ for two different sets of parameters $(c_0 = -1.5, c_2 = -0.5)$ and $c_0 = c_2 = -1$, which correspond to the state with $m = 0$ and the state with $m = 1$ given by Eq. (5) with the ansatz (14), respectively. Here the parameters in Eq. (14) calculated by the VA are $a = 0.2877$, $k = 1.0120$, and $A = 0.2723$ for the state with $m = 0$ and $a = 0.1816$, $k = 1.0041$, and $A = 0.2173$ for the state with $m = 1$. One can see that numerical wave functions are nearly identical to the VA counterparts, except for a slight mismatch at peaks and valleys. The reasons can be summarized in three aspects. First, the variational solution (14) can be reduced to the linear exact solution (9) at $a = 0$ and so is an exact solution in the linear case ($c_{0,2} = 0$). Second, in the nonlinear case, since the truncation function is determined according to the asymptotic expression (13), the tail of the wave function can always be approximated very well by the variational solution. Finally, the nonlinear effect is positively correlated with the nonlinear coefficient $c_{0,2}$ and the amplitude of the wave functions $\psi_{1,0,-1}$. This is the reason for the mismatch between the numerical solution and the variational solution at the peaks and valleys. In the case of nonlinear coefficients $|c_{0,2}| < 6$, the mismatch is kept within the tolerable range.

It is relevant to mention that the variational method under the Gaussian ansatz for solving a similar system has been reported in Ref. [32]. It is necessary to compare the Gaussian ansatz with the Bessel ansatz in terms of ease of implementation, accuracy, and scope of application. The variational method under the Gaussian ansatz is easier to implement, in which the total energy and variational parameters for the lowest energy can be obtained analytically, while they can only be obtained numerically under the Bessel ansatz. However, the Bessel ansatz is more accurate and has wider scope of application than Gaussian ansatz. The Bessel ansatz tends to become linear exact solutions in the case of weak nonlinearity and the truncation function is used to correct the deformation caused by nonlinearity. These make the Bessel ansatz have high accuracy in both strong and weak nonlinearities. In contrast, the Gaussian ansatz lacks the oscillatory property (the property of a linear exact solution or Bessel function), which makes it applicable only to the case of relatively strong nonlinearity ($|c_0| > 4$) and will make it fail in the case of weak nonlinearity ($|c_{0,2}| < 2$). Also, an important application of the Bessel ansatz is to give the phase diagram of the ground-state vortex (see Fig. 2), which is impossible for the Gaussian ansatz due to the limitation of the scope of application. In conclusion, the results given by the VA under the Bessel ansatz can be better used to study the dynamics and topological properties of the vortex ground state.

Now, by means of the results of the VA under the Bessel ansatz, we discuss the stability of the vortex ground state by employing linear stability analysis and direct simulation, respectively. The linear stability analysis can be performed by adding a perturbation to the stationary vortex solution $\psi(x, y)$ for Eq. (4),

$$\Phi(x, y, t) = e^{-i\mu t}[\psi(x, y) + w(x, y)e^{\lambda t} + v^*(x, y)e^{\lambda^* t}], \quad (16)$$

where $w(x, y)$ and $v(x, y)$ are small perturbation vectors, λ is the eigenvalue, and the asterisk stands for the complex conjugation. Substituting Eq. (16) into Eq. (1) and linearizing with respect to the perturbations, we arrive at the linear eigenvalue problem

$$\begin{pmatrix} L_1 & L_2 \\ L_2^* & L_1^* \end{pmatrix} \begin{pmatrix} w \\ v \end{pmatrix} = \lambda \begin{pmatrix} w \\ v \end{pmatrix}, \quad (17)$$

where $L_1 = i\nabla_\perp^2/2 + \beta(F_y\partial_x - F_x\partial_y) + i\mu - ic_0(\psi^\dagger\psi + \psi\psi^\dagger) - ic_2(\mathbf{F}\psi \cdot \psi^\dagger\mathbf{F}^\dagger + \psi^\dagger\mathbf{F}\psi \cdot \mathbf{F})$ and $L_2 = -ic_0\psi\psi^T - ic_2\mathbf{F}\psi \cdot \psi^T\mathbf{F}^T$. Notice that L_1 and L_2 are 3×3 matrices. Equation (17) can be solved by employing numerical simulation. The vortex solution $\psi(x, y)$ is linearly unstable by decaying or rising exponentially if λ contains a real part; otherwise it is linearly stable as complex exponential oscillation with a small perturbation does not influence the

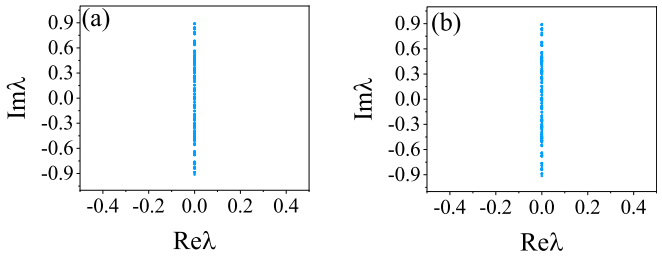

FIG. 4. Eigenspectra of the linear stability analysis for (a) $c_0 = -1.5$ and $c_2 = -0.5$, with $m = 0$, and (b) $c_0 = c_2 = -1$, with $m = 1$.

stability of $\psi(x, y)$. Figure 4 presents the eigenspectra of the linear stability analysis for two different sets of parameters shown in Fig. 3. From it one can see that their eigenspectra hardly contain the real part and so the states with $m = 0$ and 1, as the vortex ground states, are linear stable. Furthermore, we demonstrated their perturbed dynamics by dint of direct simulations of Eq. (1), and the results are summarized in Fig. 5. As predicted by linear stability analysis, the vortex ground-state solutions are stable.

The stability of Bessel vortices can be interpreted by the theory described in Ref. [39]. The radial momentum k of Bessel vortices, which corresponds to the anomalous velocity in Ref. [39], forms a centrifugal component in the density

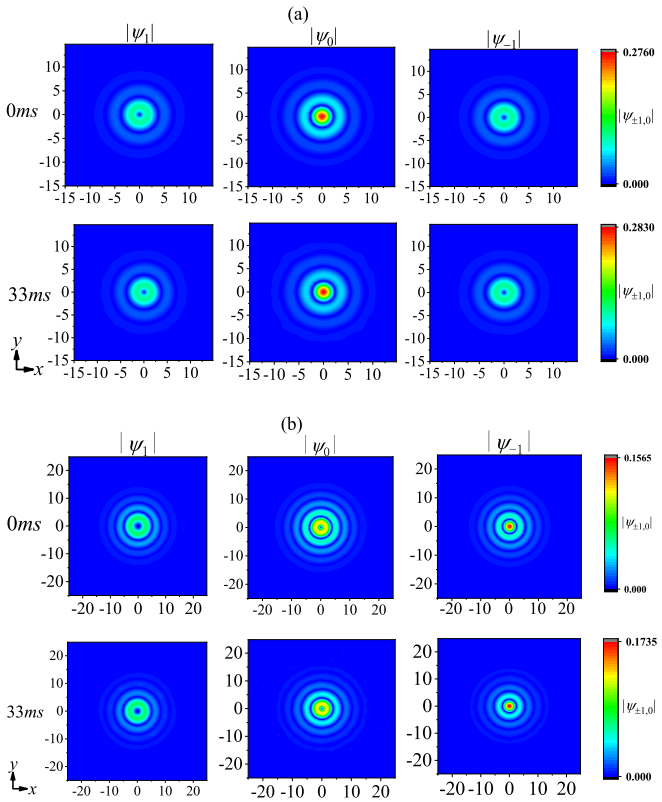

FIG. 5. Numerical evolutions of the perturbed vortex ground state with (a) $m = 0$ and (b) $m = 1$ under the initial random perturbation whose maximal value is 0.03, for (a) $c_0 = -1.5$ and $c_2 = -0.5$ and (b) $c_0 = c_2 = -1$. Here the top rows in both (a) and (b) are the initial inputs and the bottom rows are the outputs at $t = 33$ ms.

flux opposite to that arising due to the attraction between particles and prevents the collapse. Therefore, the stability of Bessel vortices can be guaranteed by balancing the attraction interaction and the spin-orbit-coupling strength.

The spin-orbit coupling in the BEC Hamiltonian is tantamount to the Dzyaloshinskii-Moriya interaction, supporting topologically nontrivial spin textures, i.e., skyrmions [40]. Here we discuss the topological properties of the vortex ground state with $m = 0$. It is found that the vortex ground state with $m = 0$ is a polar state due to $|\mathbf{S}|^2 = 0$ [41]. Also, from the eigenequation $\mathbf{n} \cdot \mathbf{F}\Phi = \delta\Phi$, where $\mathbf{n} = (n_x, n_y, n_z)$ is the unit Bloch vector, one can obtain that the eigenstate with $\delta = 0$ is of the form $\Phi_0 = ((-n_x + in_y)/\sqrt{2}, n_z, (n_x + in_y)/\sqrt{2})^T$. Thus, the vortex ground state with $m = 0$ can be written as

$$\psi = \sqrt{\rho} e^{i\vartheta} \begin{pmatrix} \frac{-n_x + in_y}{\sqrt{2}} \\ n_z \\ \frac{n_x + in_y}{\sqrt{2}} \end{pmatrix}, \tag{18}$$

where $\rho = \psi^\dagger \psi$ is the particle density and ϑ is the superfluid phase [42]. It is also invariant under simultaneous transformations $\vartheta \to \vartheta + \pi$ and $\mathbf{n} \to -\mathbf{n}$. Thus, the order parameter manifold for the polar phase can be given by $M = [\mathrm{U}(1) \times S^2]/\mathbb{Z}_2$, where U(1) denotes the manifold of the superfluid phase ϑ and S^2 is 2D sphere whose point specifies the direction of $\mathbf{n}$.

By comparing Eqs. (18) and (5) with the ansatz (14) with $m = 0$, it can be found that $n_x = \sin\Phi(r)\cos\theta$, $n_y = \sin\Phi(r)\sin\theta$, and $n_z = \cos\Phi(r)$, where $\Phi(r)$ is the polar angle of $\mathbf{n}$, $\sin\Phi(r) = -J_1(kr)/\sqrt{J_1^2(kr) + J_0^2(kr)}$, and $\cos\Phi(r) = J_0(kr)/\sqrt{J_1^2(kr) + J_0^2(kr)}$. From those expressions, one can obtain that $\mathbf{n}(r_l) = (0, 0, (-1)^l)$, where $r_0 = 0$ and r_l is the lth root of $J_1(kr) = 0$ with $l = 1, 2, \ldots$. This implies that the unit Bloch vector is pointing in the positive direction of z at the origin point and as $r = r_1$ it is pointing in the opposite direction of z. The domain covered by the vertex of the unit Bloch vector from $r = r_0$ to $r = r_1$ forms an enclosed area and can be compactified into S^2. A given mapping $\mathbf{n} : S^2 \to S^2$ determines the skyrmion topological number Q. The skyrmion topological number counts the number of times that S^2 for $\mathbf{n}$ is covered and can be calculated in a finite area where the skyrmion is restricted. For simplicity, we only consider the case of $Q = 1$, i.e., the skyrmion is restricted in the area with the boundary $r = r_1$. Thus the skyrmion can be classified by the second homotopy group $\pi_2(S^2) = \mathbb{Z}$ and characterized by topological number as the formula

$$\begin{aligned} Q = \frac{1}{4\pi} \iint_\Sigma r\, dr\, d\theta \\ \times \mathbf{n} \cdot \left[\left(\cos\theta \partial_r - \frac{\sin\theta}{r} \partial_\theta \right) \mathbf{n} \right. \\ \left. \times \left(\sin\theta \partial_r + \frac{\cos\theta}{r} \partial_\theta \right) \mathbf{n} \right], \end{aligned} \tag{19}$$

where the integral domain is $\Sigma : 0 \leqslant r \leqslant r_1, 0 \leqslant \theta < 2\pi$. The skyrmion topological number of the vortex ground state with $m = 0$ in the region of $r \leqslant r_1$ is given by $Q =$

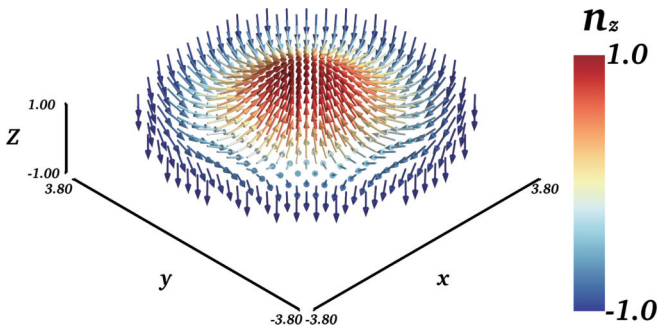

FIG. 6. Unit Bloch vector texture of the vortex ground state with $m = 0$ in the region of $r \leqslant r_1 = 3.8$, where the system parameters are $c_0 = -1.5$ and $c_2 = -0.5$.

$-0.5 \cos \Phi(r)|_{r=0}^{r=r_1} = -0.5 n_z|_{n_z=1}^{n_z=-1} = 1$. Figure 6 shows the unit Bloch vector texture of the vortex ground state with $m = 0$ in the region of $r \leqslant r_1 = 3.8$. From it one can see that the unit Bloch vector surrounds the sphere S^2 once, forming a skyrmion with $Q = 1$.

V. CONCLUSION

In summary, we have investigated the stationary vortex solutions in 2D Rashba SO-coupled spin-1 BECs with attractive contact interaction. The linear version of the system can be solved exactly by introducing the generalized momentum operator. The linear version solution is a set of Bessel vortices. Based on the Bessel vortices and by means of the variational approximation, we also given the solutions of the full nonlinear system. The results show that the variational results are in good agreement with the numerical results and can stably evolve, which can meet the requirements of long-time observation in experiment. We also investigated the vortex ground-state phase transition between the eigenstates with $m = 0$ and 1 and the unit Bloch vector texture of the vortex ground state with $m = 0$. It was found that the latter can form a skyrmion structure with topological number $Q = 1$.

ACKNOWLEDGMENTS

This research was supported by 111 project (Grant No. D18001) and the Hundred Talent Program of the Shanxi Province.

[1] P. Hauke, F. M. Cucchietti, L. Tagliacozzo, I. Deutsch, and M. Lewenstein, Can one trust quantum simulators?, Rep. Prog. Phys. **75**, 082401 (2012).
[2] D. Xiao, M.-C. Chang, and Q. Niu, Berry phase effects on electronic properties, Rev. Mod. Phys. **82**, 1959 (2010).
[3] M. Z. Hasan and C. L. Kane, *Colloquium*: Topological insulators, Rev. Mod. Phys. **82**, 3045 (2010).
[4] I. Žutić, J. Fabian, and S. D. Sarma, Spintronics: Fundamentals and applications, Rev. Mod. Phys. **76**, 323 (2004).
[5] Y.-J. Lin, K. Jiménez-García, and I. B. Spielman, Spin-orbit-coupled Bose-Einstein condensates, Nature (London) **471**, 83 (2011).
[6] B. M. Anderson, G. Juzeliūnas, V. M. Galitski, and I. B. Spielman, Synthetic 3D Spin-Orbit Coupling, Phys. Rev. Lett. **108**, 235301 (2012).
[7] Z. Wu, L. Zhang, W. Sun, X.-T. Xu, B.-Z. Wang, S.-C. Ji, Y. Deng, S. Chen, X.-J. Liu, and J.-W. Pan, Realization of two-dimensional spin-orbit coupling for Bose-Einstein condensates, Science **354**, 83 (2016).
[8] I. B. Spielman, Light induced gauge fields for ultracold neutral atoms, Annu. Rev. Cold Atom. Mol. **1**, 145 (2013).
[9] V. Galitski and I. B. Spielman, Spin-orbit coupling in quantum gases, Nature (London) **494**, 49 (2013).
[10] N. Goldman, G. Juzeliūnas, P. Öhberg, and I. B. Spielman, Light-induced gauge fields for ultracold atoms, Rep. Prog. Phys. **77**, 126401 (2014).
[11] H. Zhai, Degenerate quantum gases with spin-orbit coupling: A review, Rep. Prog. Phys. **78**, 026001 (2015).
[12] X.-Q. Xu and J. H. Han, Spin-Orbit Coupled Bose-Einstein Condensate Under Rotation, Phys. Rev. Lett. **107**, 200401 (2011).
[13] T. Kawakami, T. Mizushima and K. Machida, Textures of $F = 2$ spinor Bose-Einstein condensates with spin-orbit coupling, Phys. Rev. A **84**, 011607(R) (2011).
[14] B. Ramachandhran, B. Opanchuk, X.-J. Liu, H. Pu, P. D. Drummond, and H. Hu, Half-quantum vortex state in a spin-orbit-coupled Bose-Einstein condensate, Phys. Rev. A **85**, 023606 (2012).
[15] H. Sakaguchi and B. Li, Vortex lattice solutions to the Gross-Pitaevskii equation with spin-orbit coupling in optical lattices, Phys. Rev. A **87**, 015602 (2013).
[16] T. Kawakami, T. Mizushima, M. Nitta, and K. Machida, Stable Skyrmions in SU(2) Gauged Bose-Einstein Condensates, Phys. Rev. Lett. **109**, 015301 (2012).
[17] V. Achilleos, D. J. Frantzeskakis, P. G. Kevrekidis, and D. E. Pelinovsky, Matter-Wave Bright Solitons in Spin-Orbit Coupled Bose-Einstein Condensates, Phys. Rev. Lett. **110**, 264101 (2013).
[18] Y. Xu, Y. Zhang, and B. Wu, Bright solitons in spin-orbit-coupled Bose-Einstein condensates, Phys. Rev. A **87**, 013614 (2013).
[19] L. Salasnich and B. A. Malomed, Localized modes in dense repulsive and attractive Bose-Einstein condensates with spin-orbit and Rabi couplings, Phys. Rev. A **87**, 063625 (2013).
[20] Y. V. Kartashov, V. V. Konotop, and F. K. Abdullaev, Gap Solitons in a Spin-Orbit-Coupled Bose-Einstein Condensate, Phys. Rev. Lett. **111**, 060402 (2013).
[21] H. Sakaguchi, B. Li, and B. A. Malomed, Creation of two-dimensional composite solitons in spin-orbit-coupled self-attractive Bose-Einstein condensates in free space, Phys. Rev. E **89**, 032920 (2014).
[22] H. Sakaguchi, E. Y. Sherman, and B. A. Malomed, Vortex solitons in two-dimensional spin-orbit coupled Bose-Einstein condensates: Effects of the Rashba-Dresselhaus coupling and Zeeman splitting, Phys. Rev. E **94**, 032202 (2016)
[23] L. Salasnich, W. B. Cardoso, and B. A. Malomed, Localized modes in quasi-two-dimensional Bose-Einstein condensates with spin-orbit and Rabi couplings, Phys. Rev. A **90**, 033629 (2014).

[24] V. E. Lobanov, Y. V. Kartashov, and V. V. Konotop, Fundamental, Multipole, and Half-Vortex Gap Solitons in Spin-Orbit Coupled Bose-Einstein Condensates, Phys. Rev. Lett. **112**, 180403 (2014).

[25] Y. Li, Y. Liu, Z. Fan, W. Pang, S. Fu, and B. A. Malomed, Two-dimensional dipolar gap solitons in free space with spin-orbit coupling, Phys. Rev. A **95**, 063613 (2017).

[26] H. Sakaguchi and B. A. Malomed, One- and two-dimensional gap solitons in spin-orbit-coupled systems with Zeeman splitting, Phys. Rev. A **97**, 013607 (2018).

[27] Y. V. Kartashov, L. Torner, M. Modugno, E. Y. Sherman, B. A. Malomed, and V. V. Konotop, Multidimensional hybrid Bose-Einstein condensates stabilized by lower-dimensional spin-orbit coupling, Phys. Rev. Res. **2**, 013036 (2020).

[28] Y.-C. Zhang, Z.-W. Zhou, B. A. Malomed, and H. Pu, Stable Solitons in Three Dimensional Free Space without the Ground State: Self-Trapped Bose-Einstein Condensates with Spin-Orbit Coupling, Phys. Rev. Lett. **115**, 253902 (2015).

[29] B. A. Malomed, Creating solitons by means of spin-orbit coupling, Europhys. Lett. **122**, 36001 (2018).

[30] W. Han, X.-F. Zhang, D.-S. Wang, H.-F. Jiang, W. Zhang, and S.-G. Zhang, Chiral Supersolid in Spin-Orbit-Coupled Bose Gases with Soft-Core Long-Range Interactions, Phys. Rev. Lett. **121**, 030404 (2018).

[31] Y. V. Kartashov and D. V. Skryabin, Two-Dimensional Topological Polariton Laser, Phys. Rev. Lett. **122**, 083902 (2019).

[32] S. Gautam and S. K. Adhikari, Vortex-bright solitons in a spin-orbit-coupled spin-1 condensate, Phys. Rev. A **95**, 013608 (2017).

[33] S. K. Adhikari, Multiring, stripe, and superlattice solitons in a spin-orbit-coupled spin-1 condensate, Phys. Rev. A **103**, L011301 (2021).

[34] Z. Chen, Y. Li, and B. A. Malomed, Josephson oscillations of chirality and identity in two-dimensional solitons in spin-orbit-coupled condensates, Phys. Rev. Res. **2**, 033214 (2020).

[35] H.-B. Luo, B. A. Malomed, W.-M. Liu, and L. Li, Bessel vortices in spin-orbit coupled binary Bose-Einstein condensates with Zeeman splitting, Commun. Nonlinear Sci. Numer. Simul. **115**, 106769 (2022).

[36] J. C. Lagarias, J. A. Reeds, M. H. Wright, and P. E. Wright, Convergence properties of the Nelder-Mead simplex method in low dimensions, SIAM J. Optimiz. **9**, 112 (1998).

[37] L. Bergé, Wave collapse in physics: Principles and applications to light and plasma waves, Phys. Rep. **303**, 259 (1998).

[38] E. A. Kuznetsov and F. Dias, Bifurcations of solitons and their stability, Phys. Rep. **507**, 43 (2011).

[39] S. Mardonov, E. Y. Sherman, J. G. Muga, H.-W. Wang, Y. Ban, and X. Chen, Collapse of spin-orbit-coupled Bose-Einstein condensates, Phys. Rev. A **91**, 043604 (2015).

[40] X.-Q. Xu and J. H. Han, Emergence of Chiral Magnetism in Spinor Bose-Einstein Condensates with Rashba Coupling, Phys. Rev. Lett. **108**, 185301 (2012).

[41] T.-L. Ho, Spinor Bose Condensates in Optical Traps, Phys. Rev. Lett. **81**, 742 (1998).

[42] Y. Kawaguchi, M. Nitta, and Ma. Ueda, Knots in a Spinor Bose-Einstein Condensate, Phys. Rev. Lett. **100**, 180403 (2008).